JMEPEG (2011) 20:697–705
DOI: 10.1007/s11665-011-9881-8

1059-9495/$19.00

Nitinol Stent Fatigue in a Peripheral Human Artery Subjected to Pulsatile and Articulation Loading

Sean Michael Harvey

(Submitted May 15, 2010; in revised form January 24, 2011)

Nitinol self-expanding stents are used to treat peripheral occluded vessels such as the superficial femoral artery or the carotid. The complex vessel articulation requires a stent device that is flexible and kink resistant yet durable. The present study shows how the latest advances in commercially available engineering software tools permit engineering simulations of the many aspects of the Nitinol stent design and analysis. Two stent geometries are evaluated: a helical type stent design, and a more traditional straight strut, with multiple crowns design. The fatigue performance of the two stents is compared. The results show that advanced nonlinear finite element simulations and fatigue predictions of the Nitinol stent are possible today inside realistic simulated human arteries. The finite element analysis software used in this study is SimXpert, Marc, and Mentat (MSC Software, Santa Ana, CA).

Keywords constant life diagram, fatigue, finite element, nitinol, peripheral artery, stent

1. Introduction

In this study, the flat pattern stent geometry is automatically meshed and rolled. The stent is then expanded, shape set to a specified diameter, crimped inside a delivery device and positioned inside a realistic, tortuous artery. The Nitinol superelastic material model for the stent is based on the work of Auricchio and Taylor (Ref 1, 2), and a hyperelastic material model is used to represent the artery. With the stent positioned, the delivery device sheath is retracted deploying the device against the artery wall. Alternating diastolic to systolic pressures are applied to the vessel wall and the strain history is extracted for all regions of the finite element stent model for fatigue safety factor evaluation on a constant life diagram. In addition, the vessel is articulated resulting in bending, extension/ compression, and twisting of the stented artery. Fatigue safety factors are calculated and fatigue life predictions are made using a strain-life approach. Throughout the finite element simulations, the strain time history at all points in the stent is maintained.

This article is an invited paper selected from presentations at Shape Memory and Superelastic Technologies 2010, held May 16-20, 2010, in Pacific Grove, California, and has been expanded from the original presentation.

Sean Michael Harvey, MSC Software Corporation, Santa Ana, CA. Contact e-mail: sean.harvey@mscsoftware.com.

2. Materials and Methods

2.1 Stent Models

In the current study, two stent designs are evaluated, a helical design and a more traditional nonhelical stent design with straight struts connected by rounded crowns, and interconnected via *z* links. The helical stent design is based on an actual stent design that underwent in vivo animal and human trials. Due to the sensitive nature of the actual design, the design used in these simulations has been altered to be a rather simple repeating triangular design in a helical configuration. This was chosen as to not reveal the proprietary nature of the actual stent design. It should be noted that there are currently several FDA approved stents with some form of a helical design element on the market. The nonhelical stent design is a generic design that has too been altered to not infringe with any actual stent designs. Although the stent designs used in this study are noncommercial, the relative results that were obtained were very similar to the actual commercial designs when comparing helical and nonhelical stents deployed in arteries subjected to articulation.

The helical stent design's flat pattern curves are created using CAD. A surface is created from the curve boundaries. The preprocessor takes the surface and automatically generates a rolled cylindrical three-dimensional mesh of the desired diameter and thickness, in this case 5 mm OD and 0.0038″ (0.097 mm) thick. The element topology is an 8-node hexahedral 3D continuum element. This mesh represents the post laser cutting and electropolishing of the Nitinol stent. The shape-memory superelastic material model is based on the work of Auricchio and Taylor (Ref 1, 2). The Nitinol constitutive parameters (Ref 3) used in the simulations are shown in Table 1.

A rigid surface is introduced inside the stent and expands the device from a 5 to 6 mm OD. The 6 mm OD stent is then used strain free in the subsequent simulations. Cutting at 5 mm and expanding to 6 mm assures the stent will exhibit dynamic interference up to 6 mm, and exhibit close to the desired

Table 1 Nitinol superelastic constitutive parameters

Description	Value
Young's modulus—martensite	47,800 MPa
Young's modulus—austenite	51,700 MPa
Poisson's ratio	0.3
Start of transformation (loading)	600 MPa
End of transformation (loading)	670 MPa
Start of transformation (unloading)	288 MPa
End of transformation (unloading)	254 MPa
Transformation strain	0.063

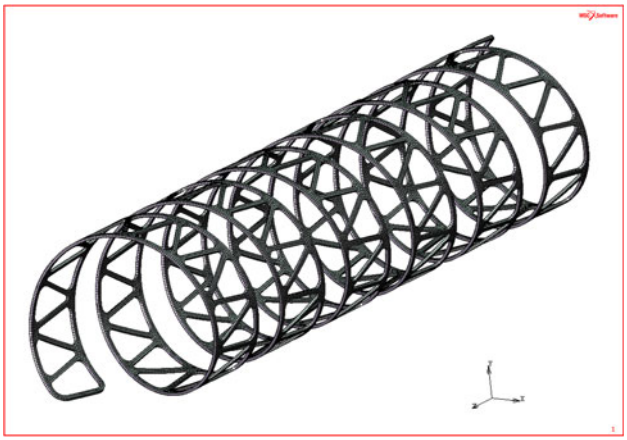

Fig. 1 6 × 26 mm helical stent mesh

designed strut pattern configuration between 5 and 6 mm. Since the helical stent unwinds during expansion, and the strut patterns do not typically deform like a standard diamond shape stent, no large expansion ratio is required to open a typical diamond-shaped strut pattern. The material properties used during the shape setting was superelastic Nitinol. The reasoning for this is as such; this helical stent design sees little straining during the expansion, as the device unwinds, unlike the typical diamond-shaped stent. Since little to no plasticity is experienced during expansion, there is no need to specify a plasticity material model. Furthermore, the stent is annealed in the simulation software which effectively erases all prior stresses and strains, and their respective histories. The stent is held at 6 mm during this process thereby resulting in a 6 mm stress/strain free stent. The length of stent used in the study is 26 mm, and is shown in Fig. 1. The simulations generally take extensive computation time, and smaller stents lengths were chosen in order to develop and prepare results for comparison in a timely manner.

The same procedure is repeated for the nonhelical stent creating the finished 6 × 29 mm stent of 0.004″ (0.102 mm) thickness, as shown in Fig. 2.

2.2 Vessel Models

Two vessel models are used in this study. The first model is a constant diameter straight tube of 4.97 mm ID, 0.7 mm wall thickness, and 47 mm in length. The tube is meshed with 8-node 3D solid hexahedral elements. This model is used to evaluate the stent deployment in vitro, comparable to physical stent testing devices, and to assess the stent behavior without

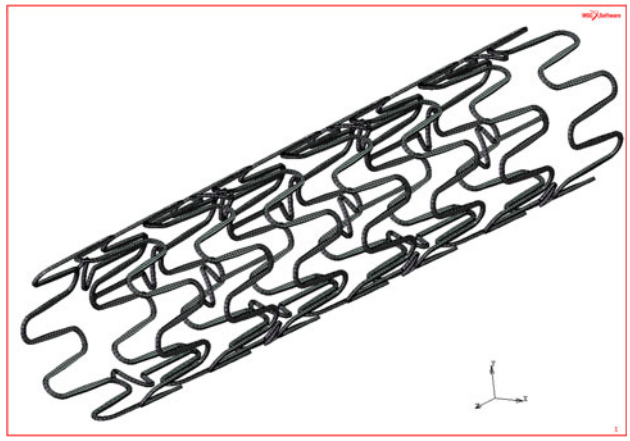

Fig. 2 6 × 29 mm nonhelical stent

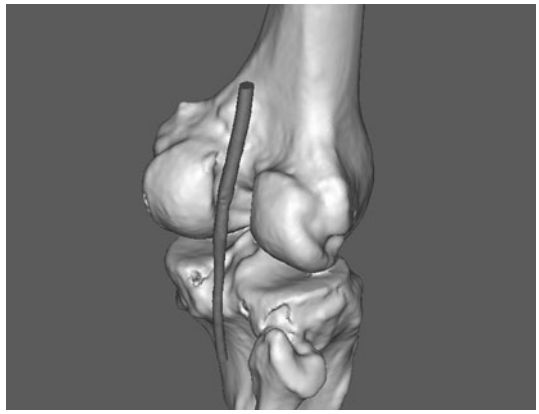

Fig. 3 Portion of SFA used in this study. Note location with respect to human knee

the added variability of the more realistic vessel representation discussed next. The second vessel used in the study is generated from CT angiography (CTA) scans of the right leg of a 68-year-old male human subject, as shown in Fig. 3. The unoccluded superficial femoral artery (SFA) at the knee is the region of interest. An unoccluded vessel is one that does not have any blockage or plaque buildup. Although the purpose of stenting is to generally open an occluded vessel, and help prevent restenosis, inclusion of the plaque buildup finite element representation would add even further complexity to a non-trivial numerical simulation and was not included as part of this study. The SFA is an artery that sees significant articulation, and is a challenge to stent successfully as the device must be compliant and fatigue resistant, and to date, a large percentage of stents deployed in the SFA experience premature fatigue failure. That is changing with the advent of more flexible stent devices. The CTA scan data is processed and segmented using Mimics software (Materialise, Ann Arbor, MI) to generate a triangular mesh of the vessel inner wall surface, which is brought into the finite element preprocessor as (stereo lithography format) STL triangles. From this triangular surface mesh, a smoothed, 4-noded quadrilateral surface mesh is constructed using a mesher that uses the existing surface mesh as the topology for the new quadrilateral surface mesh. The quadrilateral surface mesh is expanded 0.68 mm normal to the surface

forming 8-noded hexahedral 3D continuum elements. The vessel inside diameter varies from 4.9 to 6.2 mm. The length of the vessel segment used in the analysis is 61 mm. A two-term Mooney-Rivlin hyperelastic material model is specified for both vessels. The vessel is calibrated to be 5% compliant per 100 mmHg as measured on the vessel interior wall. The resulting Mooney-Rivlin coefficients used for the study are C10 = 0.221 MPa and C01 = $1.33E{-}2$ MPa. It is noted that during the CTA scan, the vessel has internal pressure. To later apply diastolic and systolic pressures to the vessel interior wall would, in essence, account for the pressure twice, and result in a vessel diameter in simulation that exceeds the size during the CTA scan. To account for this, the following procedure is adopted. The mean pressure on the vessel interior wall is calculated to be the average of the diastolic and systolic pressure.

$$p_{\text{mean}} = \frac{(p_{\text{dia}} + p_{\text{sys}})}{2} = \frac{(80\ \text{mmHg} + 160\ \text{mmHg})}{2} = 120\ \text{mmHg}$$

Then, using the vessel compliance of 5% per 100 mmHg, the vessel is scaled down about its axis. The axis is formed by extracting the vessel inside diameter cross section at multiple locations, finding the center points of these diameters, then creating a curve through these points. That is considered the vessel axis. The vessel is scaled via the equation;

$$\phi'_{\text{ID}} = \phi_{\text{ID}} * \left(1 - \left(\frac{0.05}{100\ \text{mmHg}} * p_{\text{mean}}\right)\right)$$

During the application of the diastolic and systolic pressure cycles, the mean vessel pressure of 120 mmHg will result in the vessel returned to it as measured in vivo size.

2.3 Simulation Setup: Helical Stent

The helical shape set stent is positioned inside the straight vessel with a rigid cylindrical contact surface representing the catheter ID. The catheter position and diameter are controlled via tabular input. The catheter surface is contracted to a diameter of 4.7 mm. The reasoning for this chosen diameter is as follows. Since the helical stent design used in the simulation had a simple generic triangle-shaped pattern with few struts, as to not disclose the proprietary strut pattern of the actual commercial stent design on which it was based, the stent became unstable as the stent was crimped, and the stent experienced buckling of the struts as the SMA transitioned from austenite to martensite. This could not be prevented at diameters below 4.7 mm with the chosen stent design, so for the purpose of the study, the 4.7 mm diameter was used. By not including the proper crimp, the overall results and relative comparative conclusion with the nonhelical stent design does not change, rather in the absolute sense, our results could be expected to be a bit different if the crimp to 3 mm succeeded. Since superelastic SMAs exhibit different loading and unloading curves, it is generally important to include the proper crimp, before deploying the stent in the simulation, to capture the proper path-dependant nature of the stress-strain response of the material. It was interesting and informative to predict this buckling, for if this was an actual commercial design, the simulation would predict an event that would be hard to determine otherwise, hence necessitating a design change before manufacturing an actual device. Following the crimp to 4.7 mm, the catheter is then translated along the axis of the vessel, sliding on the stent, and the stent comes into contact

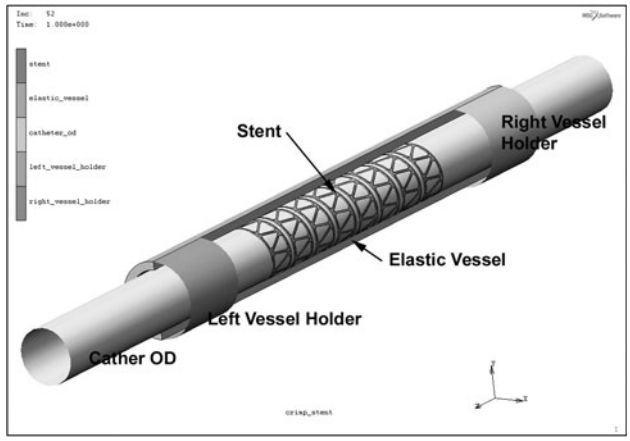

Fig. 4 Helical stent simulation setup

(apposition) with the vessel inner wall, effectively deploying the stent inside of the vessel. Friction is not considered for the stent to catheter contact, or the stent to vessel contact. During the deployment, the stent is held in the direction of the vessel axis at a single location. This is the only boundary condition on the stent and is required to prevent the stent from moving along with the catheter during deployment. The vessel is held on the outer wall at opposing ends via rigid contact surfaces. The rigid surfaces can articulate in all six degrees of freedom, affecting extension, bending, and twisting. Internal pressure loads of 80-160 mmHg (diastolic and systolic, respectively) are applied to the faces of the vessel inner wall elements for the pulsatile fatigue evaluation. The simulation setup is shown in Fig. 4. The vessel in shown cutaway to provide improved clarity to the simulation setup.

2.4 Simulation Setup: Nonhelical Stent

The nonhelical shape set stent is positioned inside the SFA vessel mesh. The catheter in this instance is represented via a flexible shell mesh. Differential orthotropic thermal expansion is used to control the catheter diameter, and not affect its length. The catheter mesh is used for both crimping of the stent, and for deployment into the vessel. The catheter diameter is reduced from 6 mm down to the fully crimped 3 mm. The catheter motion is governed by tabular input extracted from a 3D spline curve that runs down the axis of the SFA. The axis is the same axis as reference to in section 1.2. The catheter ends and two interior locations are constrained to this 3D curve via RBE2 constraint equations to control nodes that lie on the 3D spline curve. Motion of the control nodes, pulls along the catheter, and allows the catheter to navigate the vessel. Holding the stent from axial motion at a single location, the catheter is then translated along the axis of the vessel, sliding on the stent, and the stent comes into contact (apposition) with the vessel inner wall, effectively deploying the stent inside of the vessel. Friction is not considered for the stent to catheter contact, or the stent to vessel contact. The vessel is held on the outer wall at opposing ends via rigid contact surfaces. The rigid surfaces can articulate in all six degrees of freedom, affecting extension, bending, and twisting. Internal pressure distributed loads of 80-160 mmHg (diastolic and systolic, respectively) are applied to the faces of the vessel inner wall elements for the pulsatile fatigue evaluation. The simulation setup is shown in Fig. 5. The vessel in shown cutaway to provide improved clarity to the

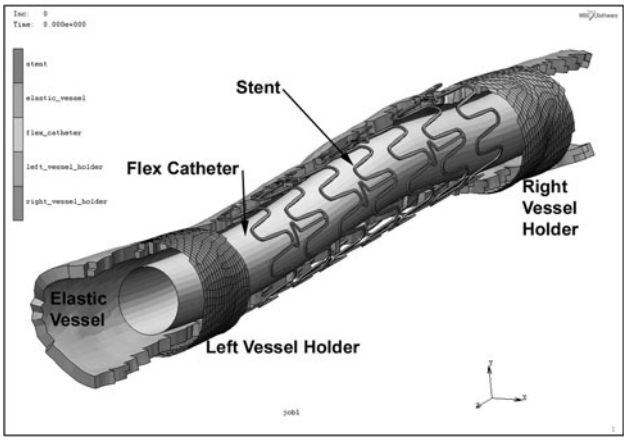

Fig. 5 Nonhelical stent simulation setup

simulation setup. Due to the nonstructured mesh pattern of the vessel, there is no clean boundary when selecting elements of the vessel to hide from view, resulting in a jagged appearance. This strictly affects model visualization.

2.5 Vessel Pulsatile Loading and Fatigue Safety Factors

The vessel interior pressure is increased to 80 mmHg, and then again to 160 mmHg with the stent deployed in the artery. The change in pressure causes the vessel to dilate, affecting a change in strain in the Nitinol stent. A Python routine is used in conjunction with the results database to extract the tensor of total strain components for the diastolic and systolic loading conditions. These equations are evaluated for the three normal and the three shear strains. Tensor shear strain and not engineering shear strain must be used in the equations.

$$\varepsilon_{ij_{\text{mean}}} = \frac{\left(\varepsilon_{ij_{\text{dia}}} + \varepsilon_{ij_{\text{sys}}}\right)}{2}$$

$$\varepsilon_{ij_{\text{alt}}} = \left|\frac{\left(\varepsilon_{ij_{\text{dia}}} - \varepsilon_{ij_{\text{sys}}}\right)}{2}\right|$$

The equivalent mean and equivalent alternating strain amplitude (Ref 4, 5) at every integration point of every element of the Nitinol stent are calculated

$$\varepsilon_{\text{m}} = \left(\varepsilon_{11_{\text{mean}}} + \varepsilon_{22_{\text{mean}}} + \varepsilon_{33_{\text{mean}}}\right)$$

$$\varepsilon_{\text{a}} = \frac{\sqrt{\left(\varepsilon_{11_{\text{alt}}} - \varepsilon_{22_{\text{alt}}}\right)^2 + \left(\varepsilon_{22_{\text{alt}}} - \varepsilon_{33_{\text{alt}}}\right)^2 + \left(\varepsilon_{33_{\text{alt}}} - \varepsilon_{11_{\text{alt}}}\right)^2 + 6\left(\varepsilon_{12_{\text{alt}}}^2 + \varepsilon_{23_{\text{alt}}}^2 + \varepsilon_{31\text{alt}}^2\right)}}{\sqrt{2} * (1 + \nu)}$$

The equivalent mean and alternating strains are then plotted on a constant life diagram and compared to the 10^7 fatigue strain limit (Ref 6), to determine if the stent can withstand the loading condition for the specified number of cycles. The routine creates a results file for graphic display of safety factor contoured on the Nitinol stent. The safety factor (Ref 6) is calculated as

$$\text{SF} = \frac{\varepsilon_{\text{allow}}}{\varepsilon_{\text{a}}}$$

where

$$\varepsilon_{\text{allow}} = \pm 0.4\% \ (10^7 \text{ Cycles})$$

A safety factor < 1 indicates that the particular region of the stent will fail in $< 10^7$ cycles. A safety factor > 1 indicates that the particular region of the stent will fail in $> 10^7$ cycles. For all safety factor calculations performed in this study, the mean strain is not accounted for due to research (Ref 6, 7) that indicates the constant life diagram of superelastic Nitinol does not exhibit the negative slopes that are traditionally seen in linear elastic engineering materials. Although the fatigue criteria may seem quite simplistic, in that only the alternating strain is compared to an allowable, without regard for the mean strain, this is consistent with the latest presentations and discussions at the SMST 2010 conference. It has been proposed at SMST 2010 (Brian Berg, BSC) that plotting alternating strain against the martensite volume fraction on the horizontal axis, may prove to be insightful. The ability of superelastic shape-memory alloys to exhibit an apparent alternating strain allowable improvement at higher mean strain is speculated to be due to strain accommodation from stress-induced martensitic transformation. The creation of such plots from fatigue tests would be of interest, as the finite element software tracks martensite volume fraction, and comparable plots could be made from simulation. It should be noted that the $\varepsilon_{\text{allow}}$ referenced above is a mean value and does not include any reduction factors such as a reliability reduction factor due to statistical scatter, etc.

2.6 Vessel Articulation and Fatigue Safety Factors

For both the straight and realistic SFA stented vessels, the vessel is articulated to simulate in vivo loading in order to quantify the behavior of the stent and evaluate the fatigue life of the device (Ref 8). The first loading condition is to axially strain the vessel 5%. The second loading condition bends the vessel a total of 32° for the nonhelical stent and to 48° for the helical stent. The different values of bending for the two different stent designs is due to the challenges in obtaining results at higher bending angles with the less compliant nonhelical stent design. The center of rotation for the articulation is offset from the axis of the vessel such that bending introduces compression in the vessel. This is shown in Fig. 6 where the center of rotation is shown as a black circle, and the bending rotation as a curved arrow. One can see from this figure the bent vessel, and how the bending introduces axial foreshortening into the vessel. The horizontal lines on both ends of the vessel mark the original position of the rigid surfaces used for the vessel articulation. This simulation setup is similar that of the physical setup of Fig. 3 in Ref 8. The third

Fig. 6 Vessel bending and twist center of rotation

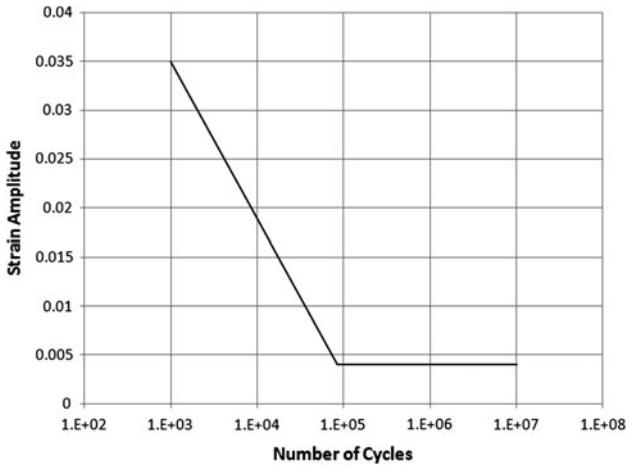

Fig. 7 Strain-life plot (Ref 6)

loading condition is to twist the now bent vessel 20°, 10° per end. This is illustrated in Fig. 6 where the twist vector is shown as double-tipped arrow with respect to the center of rotation. The fatigue safety factor is calculated and reported for bending and twisting using the same procedure as described above. Throughout the bending and twisting, the vessel internal pressure is kept constant at 160 mmHg.

2.7 Fatigue Life Predictions

If the fatigue safety factor is calculated to be <1.0, then the number of cycles to failure is $<10^7$. In these instances, it is helpful to report the predicted cycles to failure using the strain-life plot (Ref 6), which is reproduced here in Fig. 7. The plot has two regions, the low cycle region and the high cycle region. The low cycle region curve has the equation of the form.

$$\varepsilon_a = A(2N_f)^b,$$

where ε_a is the alternating strain amplitude, N_f is the cycle to failure, b −0.49, and A 1.455.

It is noted that the value for b is reported in (Ref 6), but the value of A is estimated from the referenced strain-life plot, and is subject to engineer interpretation. The high cycle region of the curve is the fatigue strain limit of 0.4%. The Python routine

Table 2 Stent fatigue prediction summary

Stent configuration	Fatigue safety factor	Predicted cycles to failure
Helical—pulsatile	2.66	$>10^7$
Helical—bending—48°	1.58	$>10^7$
Helical—twisting—20°	1.39	$>10^7$
Nonhelical—pulsatile	0.76	19,500
Nonhelical—bending—32°	0.42	4070
Nonhelical—twisting—20°	0.53	6310

takes the calculated strain amplitude for every integration point, and calculates the cycles to failure, N_f using the above equation. If the strain amplitude is ≤0.4%, the cycles to failure is calculated to be 10^7. For all life predictions in this study, the mean strain is not accounted for reasons discussed above. The constants used in this equation do not include any reduction factors such as a statistical reliability reduction factor, or other modifying factors, which are typically required to establish a working strain-life fatigue curve. Finally, to determine the fatigue life prediction for a spectrum of loading conditions (duty cycle), one can use the well-known Miner cumulative damage rule (Ref 4).

$$B_f\left[\sum \frac{N_j}{N_{fj}}\right]_{\text{onerep.}} = 1,$$

where B_f is the repetitions to failure, N_j is the applied cycles for loading condition j, and N_{fj} is the cycles to failure for loading condition j, calculated from the strain life curve.

3. Results

3.1 Results Summary

A summary of the fatigue safety factors and predicted cycles to failure for the two stent designs is summarized in Table 2.

3.2 Helical Stent: Deployment

After deployment, the helical stent is in apposition with the vessel wall. The highest equivalent strain of 0.0066 is seen in the deployed stent. The helical stent design has a fairly low deployed mean equivalent strain due to the nature of the helical design and its ability to change diameter through winding and unwinding of the helix.

3.3 Helical Stent: Pulsatile Fatigue

The helical stent deployed in the straight vessel has a minimum safety factor from pulsatile loading of 2.66. All elements in the model have the equivalent mean strain and equivalent alternating strain amplitude plotted on the constant life diagram of Fig. 8.

3.4 Helical Stent: Bending Fatigue

The helical stent deployed in the straight vessel has a minimum safety factor from 48° of bending fatigue of 1.58. All elements in the model have the equivalent mean strain and equivalent alternating strain amplitude plotted on the constant life diagram of Fig. 9.

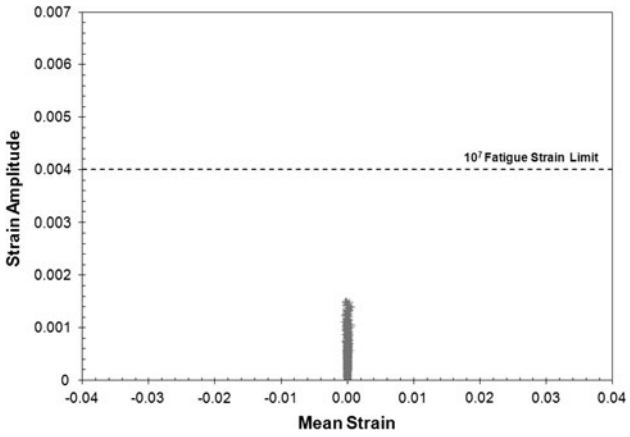

Fig. 8 Constant life diagram for helical stent subjected to pulsatile fatigue loading

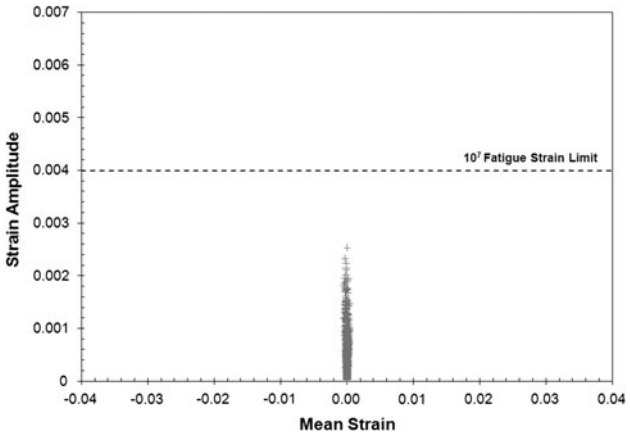

Fig. 9 Constant life diagram for helical stent subjected to 48° bending fatigue loading

3.5 Helical Stent: Twisting Fatigue

The helical stent deployed in the straight vessel has a minimum safety factor from 20° of twisting fatigue of 1.39. All elements in the model have the equivalent mean strain and equivalent alternating strain amplitude plotted on the constant life diagram of Fig. 10.

3.6 Nonhelical Stent: Deployment

The deployment of the nonhelical stent is shown in Fig. 11. The catheter is traveling to the right in the image, releasing the stent and allowing for apposition of the stent with the vessel interior wall. Again, it is noted that due to the nonstructured mesh pattern of the vessel, there is no clean boundary when selecting elements of the vessel to hide from view, resulting in a jagged appearance. The highest equivalent strain of 0.0186 is seen in the fully deployed stent.

3.7 Nonhelical Stent: Pulsatile Fatigue

The nonhelical stent deployed in the SFA has a minimum safety factor from pulsatile loading of 0.76. All elements in the model have the equivalent mean strain and equivalent alternating strain amplitude plotted on the constant life diagram of Fig. 12. With a safety factor of <1.0, a life prediction is made using the strain-life equation and plot of Fig. 7. A contour plot of the log of cycles to failure log(N_f) is shown in Fig. 13, and N_f is predicted to be 19,500 cycles to failure.

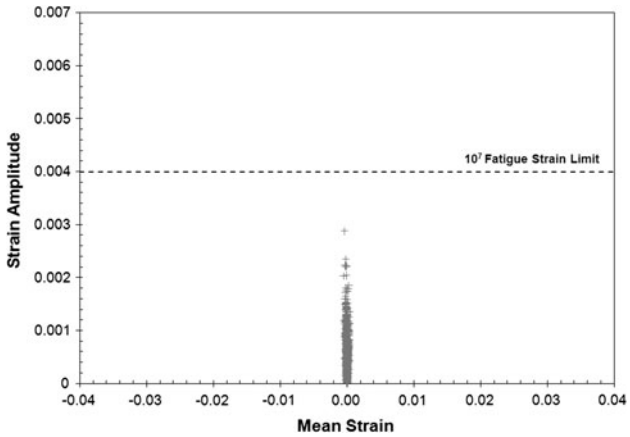

Fig. 10 Constant life diagram for helical stent subjected to 20° twisting fatigue loading

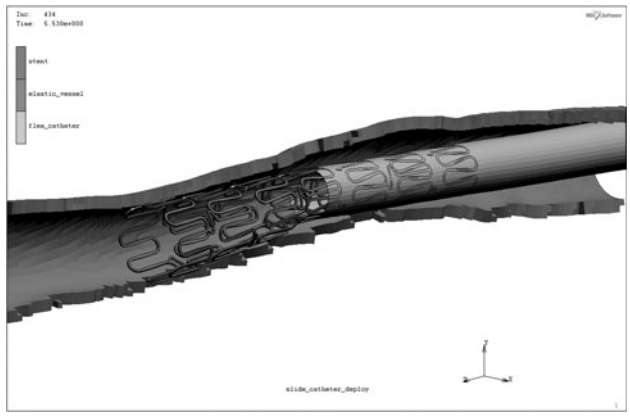

Fig. 11 Deployment of nonhelical stent in superficial femoral artery

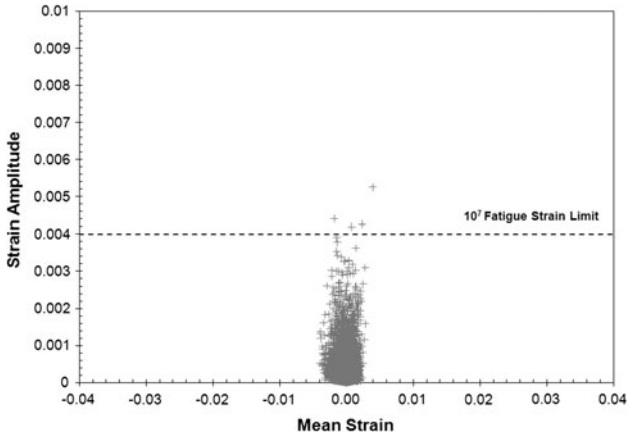

Fig. 12 Constant life diagram for nonhelical stent subjected to pulsatile fatigue loading

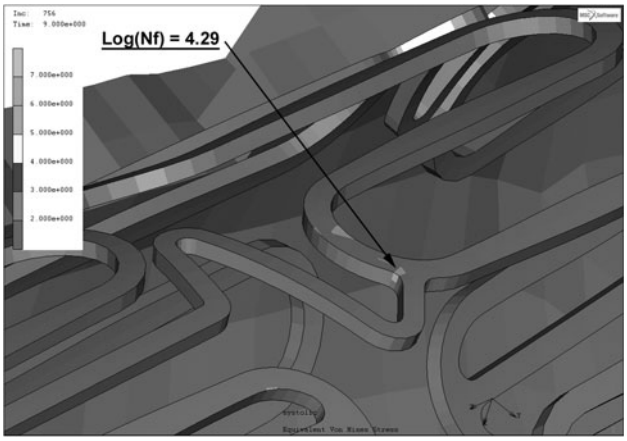

Fig. 13 Close-up of nonhelical stent with log of cycles to failure log(N_f) of critical bend subjected to pulsatile fatigue loading. log(N_f) = 4.29, N_f = 19,500 cycles to failure

Fig. 14 Nonhelical stent with safety factors contoured from 32° bending fatigue loading

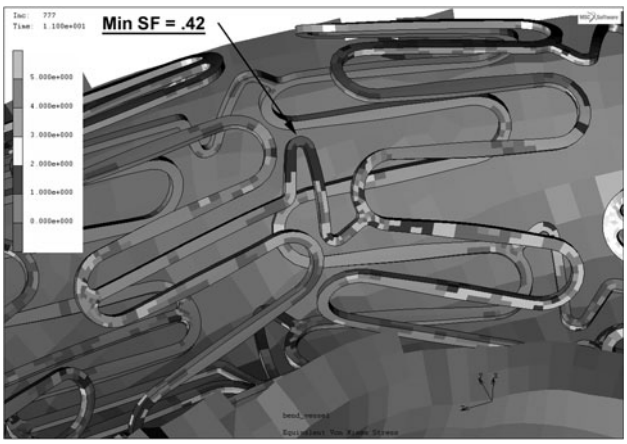

Fig. 15 Close-up of nonhelical stent with safety factors contoured from 32° bending fatigue loading. Minimum safety factor, SF = 0.42

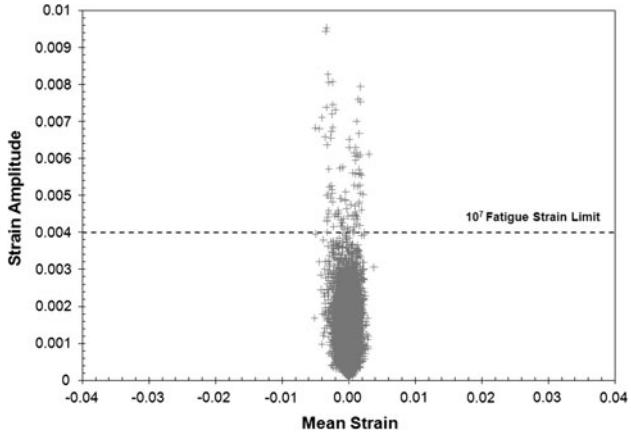

Fig. 16 Constant life diagram for nonhelical stent subjected to 32° bending fatigue loading

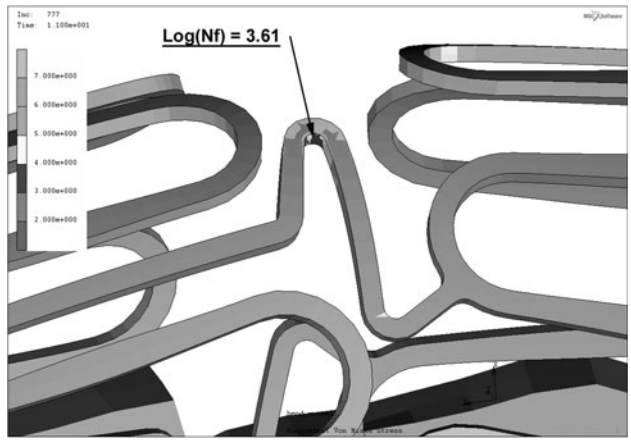

Fig. 17 Close-up of nonhelical stent with log of cycles to failure log(N_f) of critical bend subjected to 32° bending fatigue loading. log(N_f) = 3.61, N_f = 4070 cycles to failure

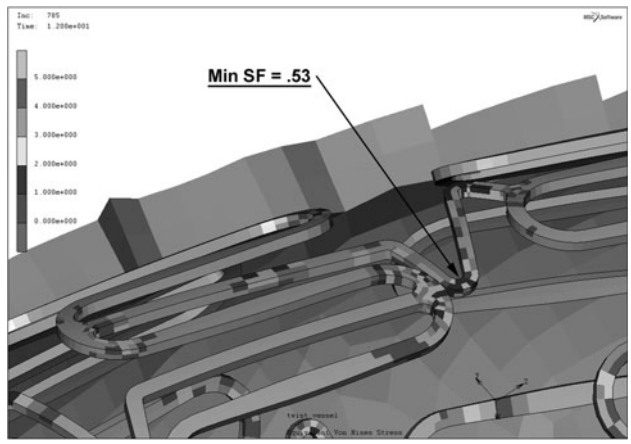

Fig. 18 Close-up of nonhelical stent with safety factors contoured from 20° twisting fatigue loading. Minimum safety factor, SF = 0.53

3.8 Nonhelical Stent: Bending Fatigue

The nonhelical stent deployed in the SFA with safety factor contours due to 32° of bending fatigue is shown in Fig. 14, with a close-up view in Fig. 15. The critical region and minimum safety factor from bending fatigue loading of 0.42 are indicated in these figures, respectively. All elements in the

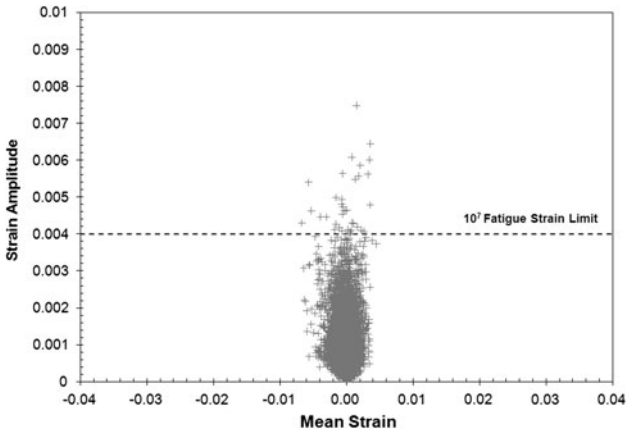

Fig. 19 Constant life diagram for nonhelical stent subjected to 20° twisting fatigue loading

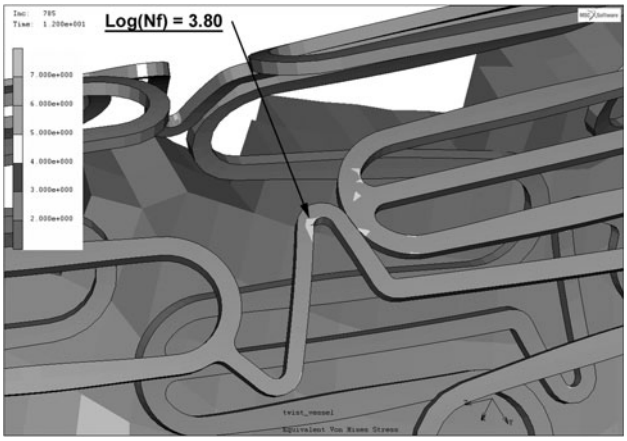

Fig. 20 Close-up of nonhelical stent with log of cycles to failure $\log(N_f)$ of critical bend subjected to 20° twisting fatigue loading. $\log(N_f) = 3.80$, $N_f = 6310$ cycles to failure

model have the equivalent mean strain and equivalent alternating strain amplitude plotted on the constant life diagram of Fig. 16. With a safety factor of < 1.0, a life prediction is made using the strain-life equation and plot of Fig. 7. A contour plot of the log of cycles to failure $\log(N_f)$ is shown in Fig. 17, and N_f is predicted to be 4070 cycles to failure.

3.9 Nonhelical Stent: Twisting Fatigue

The nonhelical stent deployed in the SFA with safety factor contours due to 20° of twisting fatigue is shown in a close-up view in Fig. 18. The minimum safety factor from twisting fatigue loading is 0.53 and is indicated by an arrow pointing to the inside radius of the *Z* link. All elements in the model have the equivalent mean strain and equivalent alternating strain amplitude plotted on the constant life diagram of Fig. 19. With a safety factor of < 1.0, a life prediction is made using the strain-life equation and plot of Fig. 7. A contour plot of the log of cycles to failure $\log(N_f)$ is shown in Fig. 20, and N_f is predicted to be 6310 cycles to failure.

4. Conclusions

In this study, successful simulations were performed of the described aspects of the deployment and service loading conditions of two Nitinol stent designs in two vessel models. The strain time history is preserved throughout the simulations and fatigue life predictions are made, facilitating the evaluation of the device performance and durability, and allowing for design changes early in the engineering design cycle. Simulated deployment into realistic peripheral arteries is feasible. These types of studies may lend insight into the nonuniform strain distributions of the stent, and potential nonapposition of the stent with the vessel wall due to the nonuniform inside diameter and tortuous nature of the realistic simulated artery. Although, stent designs with fatigue factors of safety < 1.0 are not desirable due to the high cycle requirements of these medical devices, the reporting of the predicted cycles to failure can be helpful in design studies, and simulation to test correlations. It is apparent from this study that the fatigue durability of the device is strongly dependant on the device design. For example, the inherent flexibility of the helical stent design allows for superior durability, especially in articulation loading conditions, in comparison with the nonhelical design used in this study. The nonhelical stent design used in this study, has few and finite regions (in the *Z* links) to accommodate bending, and this is clearly evident in the presented figures showing the deformed stent design. It is evident that the articulation loading conditions (bending and twisting) for these two stent design are the most critical from a fatigue standpoint, and likely explain the almost 50% fracture rates observed of some stent designs in 1 year (Ref 6). The referenced methods for calculating the equivalent alternating and equivalent mean strains (Ref 4) are just one of numerous available for the fatigue life determinations of components subject to multiaxial stresses and strains. It is the desire of the author to implement these alternative methods in future work, and compare to those implemented here. It was not the intended goal of this study to solely provide a comparison of a helical and nonhelical stent designs, and some may argue that the comparisons are not entirely fair as different vessel geometries were use, but rather to showcase a variety of stent vessel combinations and illustrate, through examples, the advances in finite element simulations and fatigue predictions for these types of medical devices.

Acknowledgments

The author would like to acknowledge Michael Lawrenchuk and Todd Pietila of Materialise for their time and expertise in creating and providing the 3D model of the superficial femoral artery that was used in this study. The author would also like to thank Dr. Kim Parnell and Doug Malcolm of MSC Software for their input and feedback during this study.

References

1. F. Auricchio, A Robust Integration-Algorithm for a Finite-Strain Shape-Memory-Alloy Superelastic Model, *Int. J. Plast.*, 2001, **17**, p 971–990

2. F. Auricchio and R.L. Taylor, Shape-Memory Alloy: Modeling and Numerical Simulations of the Finite-Strain Superelastic Behavior, *Comput. Methods Appl. Mech. Eng.*, 1997, **143**, p 175–194
3. C. Kleinstreuer, Z. Li, C.A. Basciano, S. Seelecke, and M.A. Farber, Computational Mechanics of Nitinol Stent Grafts, *J. Biomech.*, 2008, **41**, p 2370–2378
4. N.R. Dowling, *Mechanical Behavior of Materials*, Prentice Hall, Englewood Cliffs, NJ, 1993, p 378–380
5. R.I. Stephens, A. Fatemi, R.R. Stephens, and H.O. Fuchs, *Metal Fatigue in Engineering*, John Wiley & Sons, New York, 2001, p 328
6. A.R. Pelton, V. Schroeder, M.R. Mitchell, X.-Y. Gong, M. Barney, and S.W. Robertson, Fatigue and Durability of Nitinol Stents, *J. Mech. Behav. Biomed. Mater.*, 2008, **1**, p 153–164
7. A.R. Pelton, X.Y. Gong, and T. Duerig, Fatigue Testing of Diamond Shaped Specimens, *SMST-2003: Proceedings of the International Conference on Shape Memory and Superelastic Technologies*, A.R. Pelton and T. Duerig, Ed., May 5-8, 2003, Pacific Grove, SMST Society Inc., 2004, p 293–302
8. A. Nikanorov, H.B. Smouse, K. Osman, M. Bialas, S. Shrivastava, and L.B. Schwartz, Fracture of Self-Expanding Nitinol Stents Stressed In Vitro Under Simulated Intravascular Conditions, *J. Vasc. Surg.*, 2008, **48**, p 435–440